Energy Technology
Generation, Conversion, Storage, Distribution

Accepted Article

Title: Highly active cobalt/tungsten carbide@N-doped porous carbon nanomaterials derived from metal-organic frameworks as bifunctional catalysts for overall water splitting

Authors: Tao Zhao, Junkuo Gao, Jin Wu, Panpan He, Yuwen Li, and Juming Yao

To be cited as: *Energy Technol.* 10.1002/ente.201800969

Link to VoR: http://dx.doi.org/10.1002/ente.201800969

www.entechnol.de

WILEY-VCH

WILEY-VCH

DOI: 10.1002/ ((please add manuscript number))
Article type: Full Paper

Highly active cobalt/tungsten carbide@N-doped porous carbon nanomaterials derived from metal-organic frameworks as bifunctional catalysts for overall water splitting

Tao Zhao[a], *Junkuo Gao*[a,b*], *Jin Wu*[a], *Panpan He*[a], *Yuwen Li*[a], *Juming Yao*[a]

T. Zhao, Dr. J. Gao, J. Wu, P. He, Y. Li, Dr. J. Yao
[a]Institute of Fiber based New Energy Materials, The Key laboratory of Advanced Textile Materials and Manufacturing Technology of Ministry of Education, College of Materials and Textiles, Zhejiang Sci-Tech University, Hangzhou 310018, China
[b]Key Laboratory of the Ministry of Education for Advanced Catalysis Materials, Zhejiang Normal University, Jinhua 321004, China
E-mail: jkgao@zstu.edu.cn

Keywords: metal-organic frameworks; electrocatalysis; carbon materials; oxygen evolution reaction; hydrogen evolution reaction

Abstract: Currently, the design and application of low-cost and highly active bifunctional electrocatalysts for oxygen evolution reactions (OER) and hydrogen evolution reactions (HER) are still challenging. In this work, metal-organic frameworks (MOFs) were used to produce a material composed of porous nitrogen-doped carbon materials encapsulating cobalt and tungsten carbide (Co/W-C@NCNSs). Nanoscale MOFs were successfully synthesized via a microwave method and is denoted as **HZIF-W**. Moreover, the obtained MOFs were annealed under N_2 atmosphere at a temperature of 600 °C and 800 °C, and the obtained samples are designed as Co/W-C@NCNSs(600) and Co/W-C@NCNSs(800), respectively, according to the annealing temperature. The results showed that the obtained Co/W-C@NCNSs exhibit superior performance towards both the OER and HER in alkaline media. Co/W-C@NCNSs(800) had the best electrocatalytic activities, needing an overpotential of 323 mV (vs. RHE) and -252 mV (vs. RHE) to achieve a current density of 10 mA cm^{-2} for the electrocatalytic OER and HER in aqueous solution. A water electrolyzer device using Co/W-C@NCNSs(800) as both the anode and cathode only requires a cell voltage of 1.68 V to reach a current density of 10 mA cm^{-2}, illustrating that cobalt/tungsten carbide-based NCNSs derived from MOFs can be prospective materials for the electrocatalysis of water splitting.

1. Introduction

The depletion of fossil energy and serious environmental pollution have greatly hindered the development of the economy and society. Hydrogen is a clean and renewable energy that produces only water during combustion and has ample sources and a high combustion value. Water is an important material for producing hydrogen, and the production of hydrogen from water mainly contains two half-reactions: the oxygen evolution reaction (OER) and the hydrogen evolution reaction (HER). A large number of researchers are studying highly efficient electrocatalysts to increase the efficiency of water splitting.[1] In particular, IrO_2 is an excellent anodic (OER) electrocatalyst, and Pt/C is an excellent cathodic (HER) electrocatalyst.[2] However, due to the lack and high price, the large-scale production of these electrocatalysts has been limited. Therefore, it is very important to develop inexpensive and high-performance electrocatalysts. Transition metal-doped carbon materials have very good prospects for development.[3] In addition, their excellent performance and inexpensive price allow their development, among which cobalt-doped carbon is one of the most typical representatives. Cobalt- and tungsten-doped carbon materials promote the graphitization of the carbon layer during combustion, and also, the cladding of the carbon layer to the metal periphery causes stability of the metal particles and will not be consumed by the reaction in the electrolyte, resulting its good stability in acid and alkali environments.[4] Cobalt and tungsten in the cobalt-tungsten-doped carbon materials system also show metal synergy well, and they are very suitable as electrocatalysts, demonstrating a new system with excellent development prospects.[4a, 5]

Metal-organic frameworks (MOFs) have been applied to various fields, such as sensor[6], gas adsorption and separation[7], drug delivery[8], optics[9] and catalysis[10]. MOFs have a highly ordered porous structure, a high specific surface area and organic ligands that decompose into catalytic carbon layers at high temperatures, which is of great significance to improving the electrocatalytic performance of carbon materials.[11] Various types of carbon materials, including nanosheets[12], nanoparticles[13], hollow structures[14], and nanotube structures[15] have been widely reported. In particular, metal and nitrogen-doped nanocarbon materials prepared with MOFs as templates have very good electrocatalytic application prospects.[16]

Here, we designed a tungsten-carbon/cobalt embedded nitrogen-doped carbon electrocatalyst by using MOF nanocrystals (**HZIF-W**) as templates via a facile microwave synthesis method. The carbonization and combustion of **HZIF-W** was conducted at 600 ºC and 800 ºC to produce tungsten-carbon/cobalt-embedded nitrogen-doped carbon materials, as shown in Scheme 1. As expected, Co/W-C@NCNSs(800) showed outstanding overall water splitting in an alkaline solution (1.0 M KOH). We found that metallic cobalt and tungsten can provide more active sites, and the synergy between the bimetallic particles significantly improves the overall water splitting performance and still exhibits excellent stability after 1000 cycles. Using a two-electrode system, we measured the overall water splitting potential of 1.687 V (vs. RHE) in an alkaline solution (1.0 M KOH) with a catalyst of Co/W-C@NCNSs(800). This shows that Co/W-C@NCNSs(800) has an excellent overall water splitting performance and a very promising application prospect.

Scheme 1. The schematic illustration of the preparation process of nanosheets Co/W-C@NCNSs.

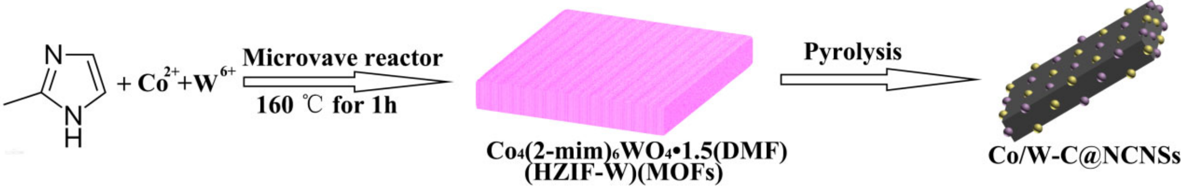

2. Results and discussion

The MOF containing both Co and W was denoted as **HZIF-W** and was similar to the structure of large single crystals first reported by Zhang's group.[17] We developed a facile microwave synthesis method and successfully obtained nanocrystals of **HZIF-W**. The pure phase of **HZIF-W** was confirmed via powder XRD, as shown in Figure S1. The morphology of **HZIF-W** was investigated via SEM, displaying a nanocrystal morphology. Then, **HZIF-W** nanocrystals were pyrolyzed at high temperatures to obtain Co/W-C@NCNSs. Powder XRD was performed to determine the phase formation process of Co/W-C@NCNSs. As shown in Figure 1, pyrolysis of the MOF leads to the formation of Co/W-C@NCNSs. In the pattern of the Co/W-C@NCNSs(800), the obvious diffraction peaks at 31.5° (001), 35.6° (100), and 48.3° (101) belong to the hexagonal WC phase, and 44.2° (111) belongs to cubic Co. The XRD pattern of Co/W-C@NCNSs(600) is shown in Figure S3, and the results show that the peak value of Co/W-C@NCNSs(600) is different from that of Co/W-C@NCNSs(800). It is shown in Figure S3 that WO_3 is present in Co/W-C@NCNSs(600), which is the result of incomplete carbonization at 600 ℃. As the sintering temperature increases, carbonization becomes more and more sufficient and WO_3 gradually changes to WC. The results of Thermogravimetric Analysis(TGA) is shown in Figure S2. As the sintering temperature increases, the quality of the catalyst decreases continuously, which is caused by the conversion of WO_3 into WC.

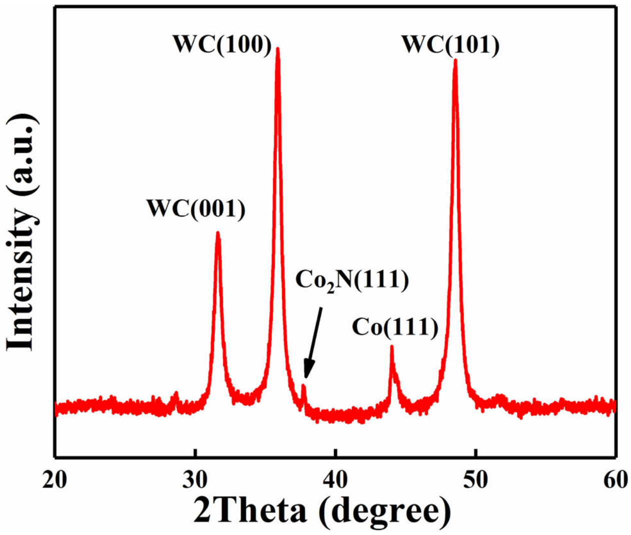

Figure 1. XRD patterns of Co/W-C@NCNSs(800).

SEM was used to examine the morphology of the synthesized Co/W-C@NCNSs samples. Figure 2a and 2b show typical SEM images of **HZIF-W** sample, and Figure 2c and 2d show typical SEM images of Co/W-C@NCNSs(800). Typical SEM images of Co/W-C@NCNSs(600) are illustrated in Figure S4c and Figure S4d. From the image, **HZIF-W** shows a nanoplate morphology with a size of approximately 300 nm. After calcination at 600 ºC and 800 ºC, the original morphology nearly remains. Figure 2e and 2f show typical TEM images of Co/W-C@NCNSs(800), and the sample exhibits an ideal structure. The graphite carbon phase formed by the carbonization of the organic ligand envelops the metal components, sufficiently protecting the metal from corrosion by the external environment and greatly improving the stability of the metal.

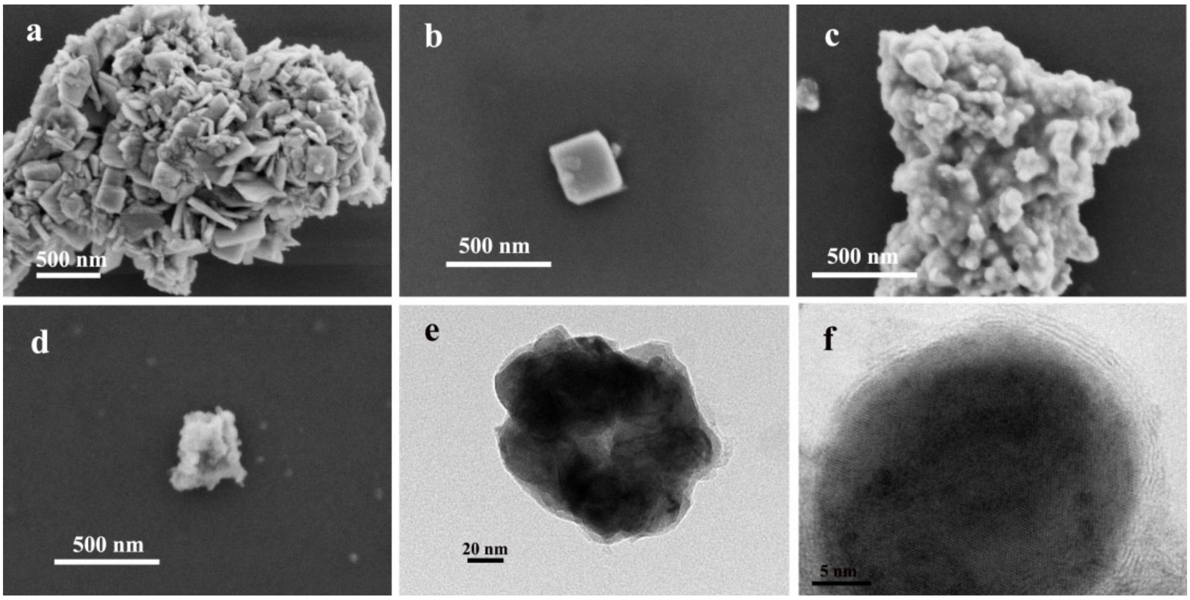

Figure 2. (a and b) SEM images of $Co_4(2\text{-mim})_6WO_4\cdot 1.5(DMF)$ (**HZIF-W**), (c and d) Co/W-C@NCNSs(800), (e and f) TEM images of Co/W-C@NCNSs(800).

The elemental composition and electronic structure of Co/W-C@NCNSs(800) were determined by X-ray photoelectron spectroscopy (XPS), whereby the surface was composed of C, Co, N, and W, the composition analysis of Co/W-C@NCNSs(800) was shown on Table S1. Figure 3a full survey results of the of Co/W-C@NCNSs(800). It shows that Co/W-C@NCNSs(800) contains elements such as W, C, Co, N and O. Figure 3b shows the high-resolution XPS C 1s spectrum. The peak at 284.5 eV is attributed to W-bonded carbon, and

10.1002/ente.201800969

the peak at 284.8 eV is attributed to the graphitic C-C. Figure 3c shows the high-resolution XPS Co 2p spectrum. The regional Co 2p spectrum reveals a high energy band at 795.7 eV (Co $2p_{1/2}$) and a low energy band at 780.5 eV (Co $2p_{3/2}$).[18] In addition, Figure 3d shows the high-resolution XPS spectrum of N 1s. Three peaks at 398.3 eV, 399.6 eV and 401.1 eV are ascribed to pyridinic-N, pyrrolic-N and quaternary-N.[19] Figure 3d shows the high-resolution XPS spectrum of W 4f with peaks at 31.7 eV and 33.7 eV, which are contributions from W-C.[5b] In addition, the represented by WC has a contribution of the W 4f peak at 35.5 and 37.6 eV.[20]

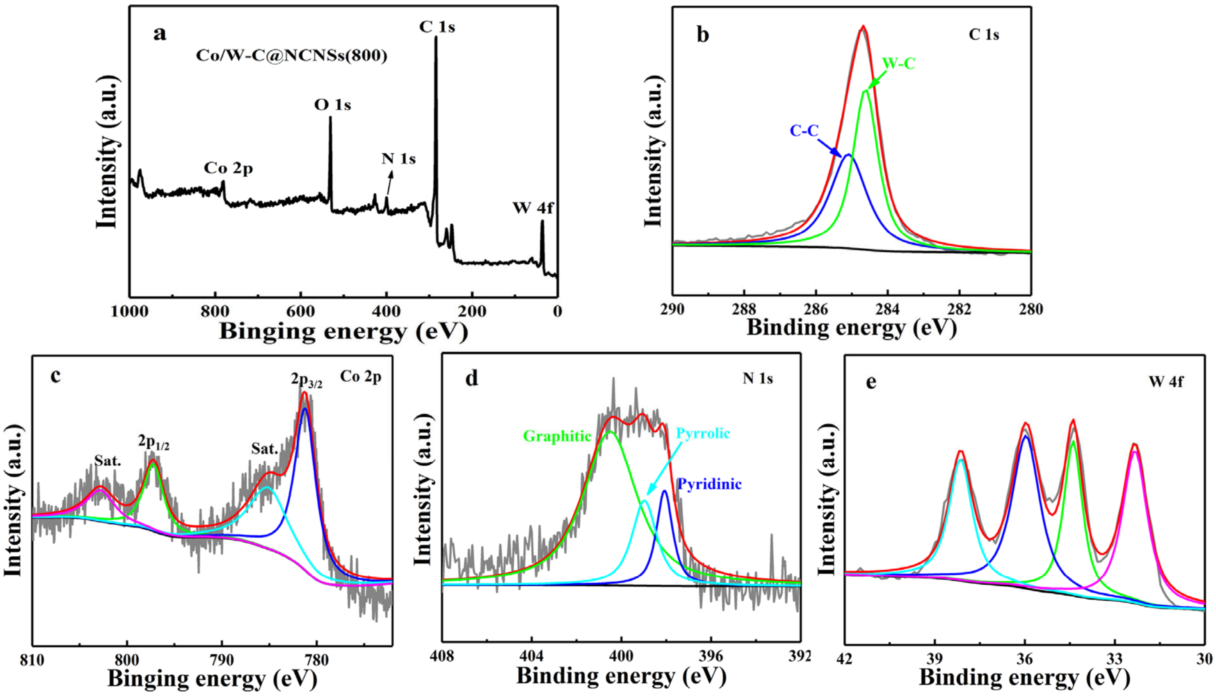

Figure 3. XPS spectra of Co/W-C@NCNSs(800): (a) full survey results of the of Co/W-C@NCNSs(800), (b) C 1s, (c) Co 2p, (d) N 1s and (e) W 4f.

The measurement of nitrogen adsorption isotherms can study the specific surface area and pore structure of Co/W-C@NCNSs. Figure 4a shows the nitrogen sorption isotherm of Co/W-C@NCNSs(600) and Figure 4b shows the nitrogen sorption isotherm of Co/W-C@NCNSs(800). Both curves show a typical type IV and hysteresis loop at a relative pressure of 0.5-1.0, which indicates the presence of micropores and mesopores in Co/W-C@NCNSs**.** The hysteresis loop of Co/W-C@NCNSs(800) is more pronounced than that of

10.1002/ente.201800969

Co/W-C@NCNSs(600), which shows that the aperture of Co/W-C@NCNSs(800) is smaller than that of Co/W-C@NCNSs(600). The specific surface area of Co/W-C@NCNSs(800) is 112 m^2 g^{-1} with pore diameter of 1.84 nm, while the specific surface area of Co/W-C@NCNSs(600) is 74 m^2 g^{-1} with pore diameter of 2.40 nm.

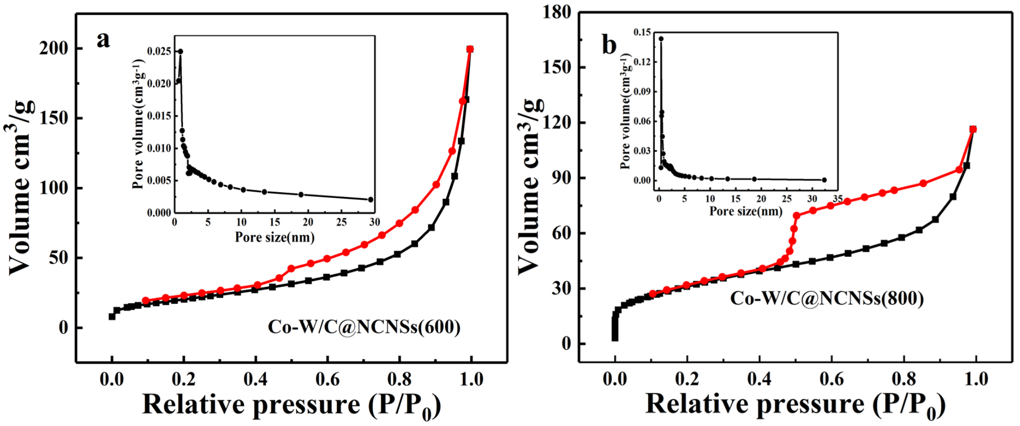

Figure 4. (a) The nitrogen sorption isotherm of Co/W-C@NCNSs(600); (b) The nitrogen sorption isotherm of Co/W-C@NCNSs(800).

The samples were drop-cast onto glassy carbon electrodes (GCE, 0.07 cm^{-2}) and electrochemical tests were carried out in a standard three-electrode system in an alkaline medium (1.0 M KOH solution). First, we measured the electrocatalytic OER activity of the Co/W-C@NCNSs. Figure 5a shows the polarization curves of the Co/W-C@NCNSs in a 1.0 M KOH solution at a scan rate of 5 mV s^{-1}. IrO_2 is used as a standard comparison sample and demands an overpotential of 300 mV (vs. RHE) to achieve a current density of 10 mA cm^{-2}. The Co/W-C@NCNSs(800) sample shows a high activity for the electrocatalytic OER and performs better than Co/W-C@NCNSs(600). This is because Co/W-C@NCNSs(800) has a more complete carbonization, higher degree of graphitization, better conductivity, and higher electron transfer efficiency. Also, Co/W-C@NCNSs(800) has a more complete carbon structure (as seen in Figure 1), a larger specific surface area, and the calculation results also show that it has a higher electrochemically active surface area (ECSA) (Supporting information), which results to its excellent performance. The Co/W-C@NCNSs(800) catalyst only demands an overpotential of 323 mV (vs. RHE) to achieve a current density of 10 mA cm^{-2}, and Co/W-C@NCNSs(600) needed 495 mV (vs. RHE), which shows that of Co/W-C@NCNSs(800) is significantly lower than that of Co/W-C@NCNSs(600). When the current density is larger than 28 mA cm^{-2}, Co/W-C@NCNSs(800) requires a lower overvoltage than IrO_2, indicating that Co/W-C@NCNSs(800) has a better catalytic performance in a high current density area. We also compared these catalysts with other electrocatalysts for OER performance and found that Co/W-C@NCNSs(800) has excellent performance, as shown in Table S2.

The electrocatalytic OER kinetics of Co/W-C@NCNSs were further studied through Tafel plots. As shown in Figure 5b, the Tafel slope of Co/W-C@NCNSs(800) is 75.5 mV dec^{-1} and is smaller than the Tafel slope of Co/W-C@NCNSs(600) (96.2 mV dec^{-1}). To gain further insight into the OER kinetics, electrochemical impedance spectroscopy (EIS) was measured for Co/W-C@NCNSs. This technique can probe relaxation processes over a large frequency domain based on the disruption method. The adsorption of a reactive intermediate (general intermediate in OER) on the electrode surface was displayed by a low-frequency semicircle, and a high-frequency semicircle corresponds to charge transfer processes. As shown in Figure 5c, Co/W-C@NCNSs(800) created a smaller semicircle radius in the high-frequency region than IrO_2, which explains that Co/W-C@NCNSs(800) had a higher charge transport efficiency than IrO_2 during the electrochemical OER process. To further test the durability of Co/W-C@NCNSs(800), LSV plots after 1000th CV cycles were recorded and are shown in Figure S5. Figure 5d shows the chronoamperometry test for Co/W-C@NCNSs at a constant potential of 1.54 V, revealing that the activity remains very good even after a 36,000 s catalytic test. SEM images (Figure S4) and XRD (Figure S6) patterns of the Co/W-C@NCNSs(800) after chronoamperometry test showed no morphological and phase changes. The OER activity demonstrated the high stability of Co/W-C@NCNSs(800) under electrocatalytic conditions.

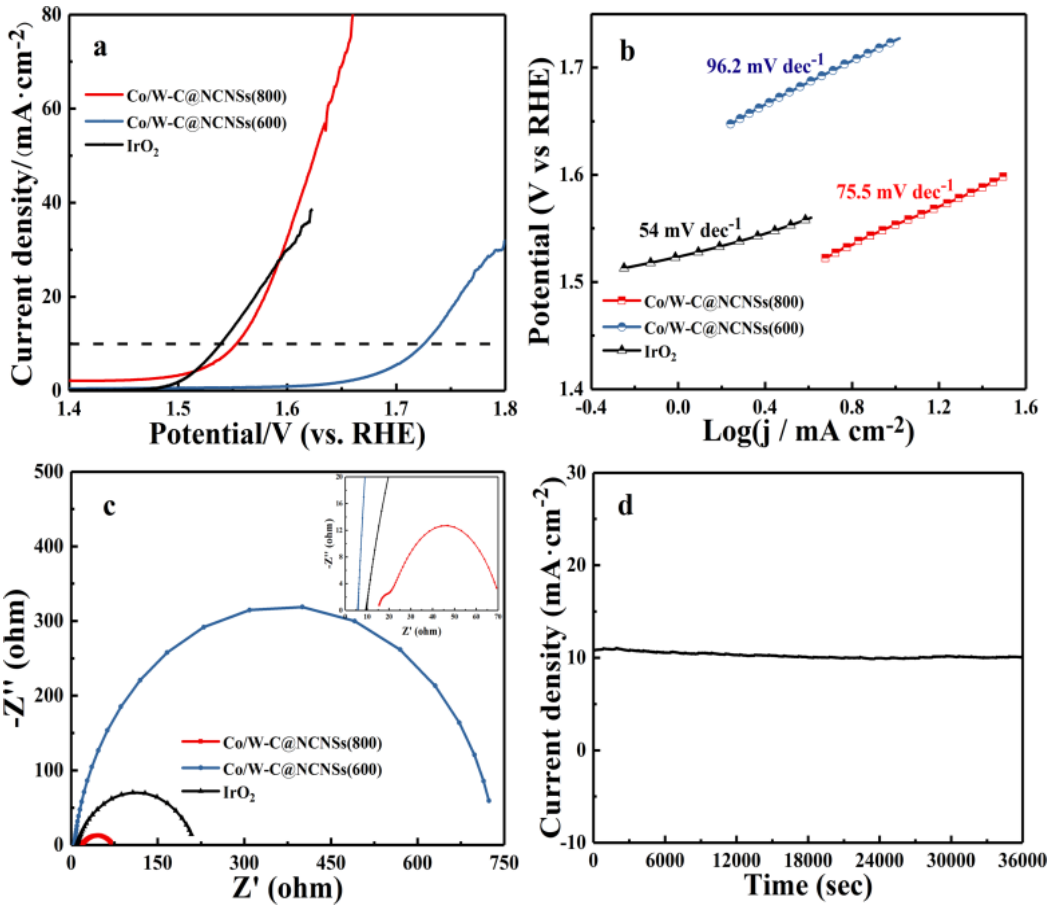

Figure 5. (a) Polarization curves of the Co/W-C@NCNSs in a 1.0 M KOH solution at a scan rate of 5 mV s^{-1} for electrocatalytic OER. (b) Tafel plots of the Co/W-C@NCNSs reference for electrocatalytic OER. (c) EIS Nyquist plots of the Co/W-C@NCNSs for electrocatalytic HER at a potential of 1.523 V. (d) The chronoamperometric measurements of Co/W-C@NCNSs(800) at 1.54 V vs. RHE.

Some previous studies have reported that tungsten carbide showed activity for the electrocatalytic HER, and most studies used acidic media, while there are few reported for used in alkaline media.[21] Here, Co/W-C@NCNSs are used for electrochemical tests in alkaline media (1.0 M KOH solution), and we further evaluate the electrocatalytic HER performance of Co/W-C@NCNSs in alkaline solutions not considering the OER and demonstrate their high activity for electrocatalytic HER. Figure 6a shows polarization curves of Co/W-C@NCNSs in a 1.0 M KOH solution at a scan rate of 5 mV s^{-1}. Similar to the electrocatalytic OER, the Co/W-C@NCNSs(800) sample shows a high activity for the electrocatalytic HER, and performs better than Co/W-C@NCNSs(600). Pt/C demands an overpotential of -96 mV (vs. RHE), and the Co/W-C@NCNSs(800) catalyst demands an overpotential of -252 mV (vs. RHE) to achieve a current density of -10 mA cm^{-2}, but Co/W-C@NCNSs(600) need -418 mV (vs. RHE). Additionally, Co/W-C@NCNSs(800) has excellent HER performance in alkaline conditions compared to that of other catalysts as shown in Table S3.

The Tafel slope estimated from the polarization curves was used to evaluate the HER kinetics. In Figure 6b, the Tafel plot of Co/W-C@NCNSs(800) is 80.1 mV dec^{-1} and that of Co/W-C@NCNSs(600) is 167 mV dec^{-1}, showing that the Tafel plot of Co/W-C@NCNSs(800) is significantly smaller than that of the Co/W-C@NCNSs(600). We measured the EIS to gain further insight into the HER kinetics. Figure 6c reveals the Nyquist plots of Co/W-C@NCNSs, which show the presence of a semicircle. Obviously, in the same potential, Co/W-C@NCNSs(800) created a smaller semicircle radius in the high frequency region than Co/W-C@NCNSs(600), which explains that Co/W-C@NCNSs(800) had a higher charge transport efficiency than Co/W-C@NCNSs(600) during the electrochemical HER process. To further test the durability of Co/W-C@NCNSs(800), LSV plots after 1000th CV cycles were recorded and are shown in Figure S7. Figure 6d shows the chronoamperometry test for Co/W-C@NCNSs at a constant potential of -0.23 V, revealing that the activity remains very good even after a 36,000 s catalytic test. It was confirmed that Co/W-C@NCNSs(800) has a very significant electrocatalytic HER stability in alkaline solutions (1.0 M KOH).

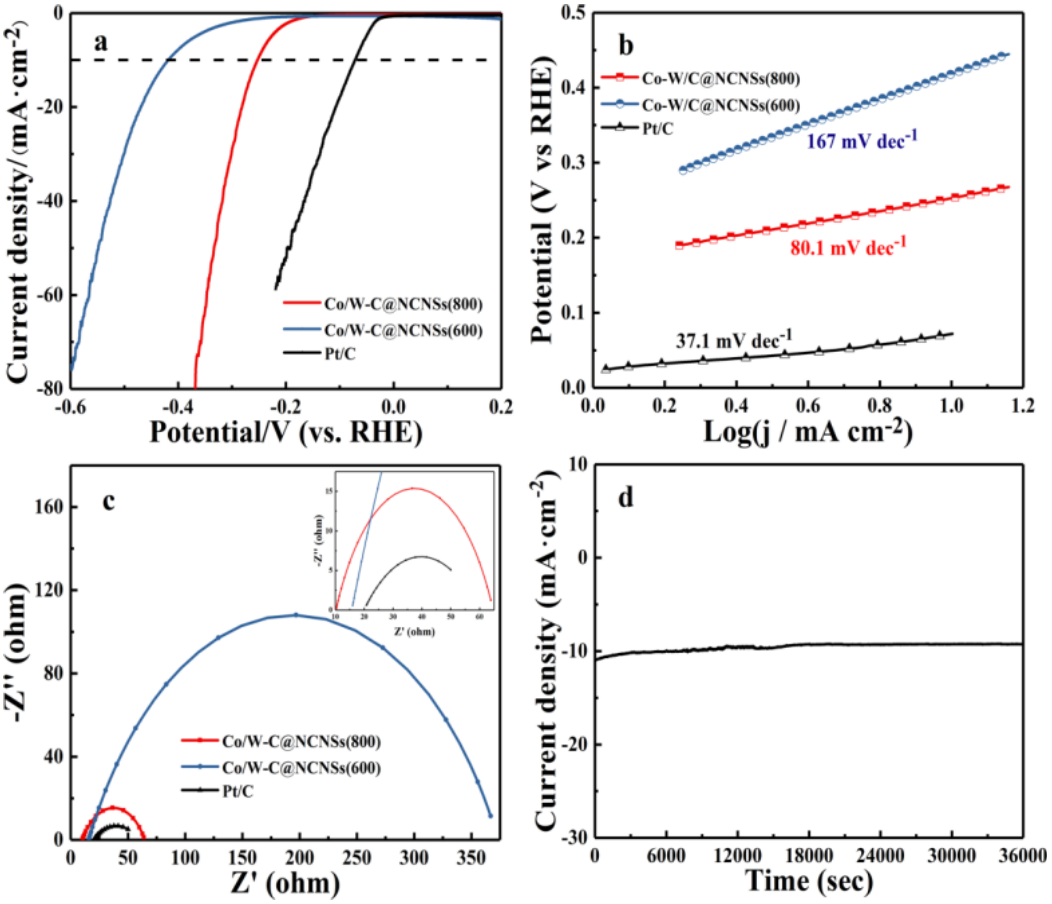

Figure 6. (a) Polarization curves of Co/W-C@NCNSs in a 1.0 M KOH solution at a scan rate of 5 mV·s^{-1} for the electrocatalytic HER. (b) Tafel plots of the Co/W-C@NCNSs reference for electrocatalytic HER. (c) EIS Nyquist plots of Co/W-C@NCNSs for the electrocatalytic HER at a potential of -0.477 V. (d) Chronoamperometric measurements of Co/W-C@NCNSs (800) at -0.23 V vs. RHE.

To further reflect the electrocatalytic performance of Co/W-C@NCNSs, the comparison of catalyst results for overall water splitting in a 1.0 M KOH solution has been illustrated in Table 1. When the current density is 10 mA cm^{-2}, the potential of the Co/W-C@NCNSs(800) for HER and OER is -0.252 V and 1.553 V, respectively, and the total potential for overall water splitting is 1.805 V. However, Co/W-C@NCNSs(600) needs a higher potential to complete overall water splitting. IrO_2 and Pt/C are regarded as the best electrocatalysts. When Pt/C was used as a catalyst, a total potential of 1.946 V was required for overall water splitting, which is larger than that of Co/W-C@NCNSs(800), meaning that Co/W-C@NCNSs(800) has a better performance than Pt/C in overall water splitting. Since Co/W-C@NCNSs(800) has excellent OER and HER activity, we further use it as a dual-functional electrocatalyst to drive overall water splitting in 1.0 M KOH. We use a two-electrode system to fully test Co/W-C@NCNSs(800) for overall water splitting, as shown in Figure 7a. As shown in Figure 7b, we found that overall water splitting reaches a battery voltage as low as 1.68 V at a 10 mA cm^{-2} current density, which is less than the calculated theoretical value of 1.80 V, and a summary of different bifunctional electrocatalysts for overall water splitting in 1.0 M KOH solution is shown in Table 2. This shows that Co/W-C@NCNPs(800) is more suitable for overall water splitting than most catalysts.

Table 1. Comparison of catalyst results for overall water splitting in a 1.0 M KOH solution.

Catalysts	E_{OER} (V vs. RHE) J = 10 mA cm^{-2}	E_{HER} (V vs. RHE) J = -10 mA cm^{-2}	Overall water splitting E (V) = E_{OER} - E_{HER}
Co/W-C@NCNSs(800)	1.553	-0.252	1.805
Co/W-C@NCNSs(600)	1.725	-0.418	2.143
IrO_2(OER),Pt/C(HER)	1.530	-0.096	1.626
Pt/C(OER),Pt/C (HER)	1.850	-0.096	1.946

Table 2. Summary of different bifunctional electrocatalysts for overall water splitting in 1.0 M KOH solution.

electrocatalysts	Substrate	Cell votages @*j*10/V	Reference
Co/W-C@NCNSs(800)	GCE	1.687	This work
Co-P/NC	GCE	~1.70	[22]
CoP/rGO	Carbon Fiber Paper	1.70	[23]
Ni_3S_2/NF	Ni foam	1.7	[24]
Ni_5P_4	stainless steel electrode	~1.7	[25]
NiCoSe2-x/NC	GCE	1.53	[26]
Co-P	GCE	1.67	[27]
Co-B@CoO/Ti	Ti mesh	1.56	[28]
CoOx@CN	Ni foam	1.55	[29]
NF-Ni_3Se_2/Ni	Ni foam	1.612	[30]

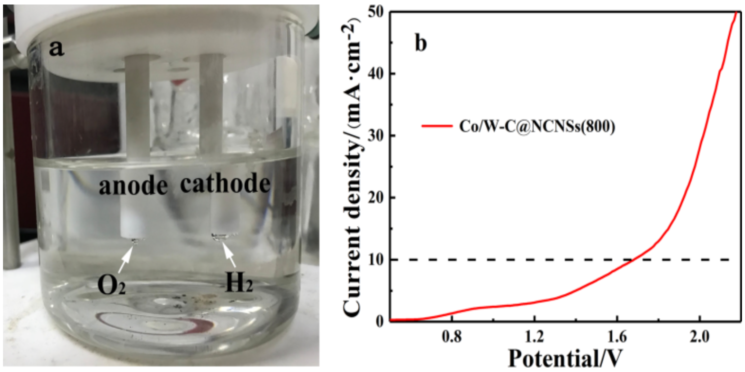

Figure 7. (a) An optical photograph of the working diagram. (b) The polarization of Co/W-C@NCNSs(800) as an anode and cathode for overall water splitting in a two-electrode system, respectively.

The ECSA of Co/W-C@NCNSs was evaluated by using cyclic voltammetry in the region of 1.00 to 1.10 vs. RHE in the non-Faradaic region to gain insight into its excellent OER performance. Figure 8a and 8b shows the CVs of Co/W-C@NCNSs(600) and Co/W-C@NCNSs(800) measured at different scan rates from 10 to 50 mV·s^{-1}. It is clear that Co/W-C@NCNSs(800) shows a higher current density, which means that the C_{dl} of Co/W-C@NCNSs(800) may be greater than that of Co/W-C@NCNSs(600). The calculated C_{dl} values for Co/W-C@NCNSs(600) and Co/W-C@NCNSs(800) were 1.68 mF cm^{-2} and 9.83 mF cm^{-2}, respectively, as presented in Figure 8c. It is clear that the C_{dl} value of Co/W-C@NCNSs(800) is significantly higher than that of Co/W-C@NCNSs(600), which indicates that Co/W-C@NCNSs(800) has a higher ECSA, which increases the functional surface of the catalytically active sites, and has more excellent bubble dissipating ability. Therefore, Co/W-C@NCNSs(800) catalyzes more excellently. Compared with Co/W-C@NCNSs(800), the electrocatalytic activity (HER and OER) of Co/W-C@NCNSs(600) is much lower, which also confirms the hypothesis.

10.1002/ente.201800969

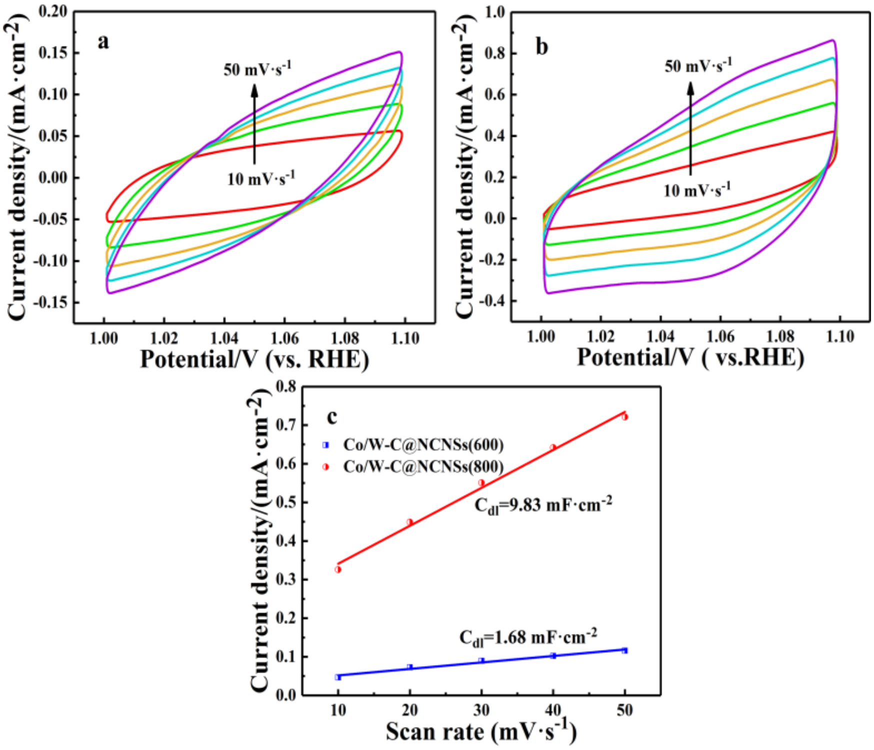

Figure 8. CVs of Co/W-C@NCNSs(600) (a) and Co/W-C@NCNSs(800) (b) measured at different scan rates from 10 to 50 mV·s-1. (c) Capacitive currents at 1.05 V against the scan rates of different samples.

3. Conclusion

In this study, tungsten-carbon/cobalt-embedded nitrogen-doped carbon electrocatalysts were fabricated using MOF nanocrystals (HZIF-W) as templates via a facile microwave synthesis method and have very excellent bifunctional electrocatalytic activity for OER and HER. It is found that Co/W-C@NCNSs(800) had a higher specific surface and more active sites, which proves that Co/W-C@NCNSs(800) has better performance than Co/W-C@NCNSs(600). The obtained results demonstrated that when the current density is 10 mA cm^{-2}, the overpotential of OER is 323 mV, and the overpotential of HER is -252 mV for Co/W-C@NCNSs(800) in alkaline media. A water electrolyzer device using Co/W-C@NCNSs(800) as both the anode and cathode only requires a cell voltage of 1.68 V to reach a current density of 10 mA cm^{-2}. Because the carbon layer offers protection, Co/W-C@NCNSs(800) can maintain very good stability when testing the HER or OER in alkaline solution, which is very conducive to large-scale development. The result illustrates that cobalt/tungsten carbide-based NCNSs derived from MOFs can be prospective new materials for electrocatalytic water splitting.

Supporting Information

Supporting Information is available from the Wiley Online Library or from the author.

Acknowledgements

This work is supported by the National Natural Science Foundation of China (51672251) and Science Foundation of Zhejiang Sci-Tech University (ZSTU) under Grant No. 13012138-Y. J. G. acknowledges the financial support from Qianjiang talents plan of Zhejiang Province (QJD1502019).

Received: ((will be filled in by the editorial staff))
Revised: ((will be filled in by the editorial staff))
Published online: ((will be filled in by the editorial staff))

References

[1] a) M. Tahir, L. Pan, F. Idrees, X. Zhang, L. Wang, J.-J. Zou, Z. L. Wang, *Nano Energy* **2017**, *37*, 136-157; b) Z. W. Seh, J. Kibsgaard, C. F. Dickens, I. Chorkendorff, J. K. Nørskov, T. F. Jaramillo, *Science* **2017**, *355*, eaad4998; c) X. Liu, L. Dai, *Nat. Rev. Mater.* **2016**, *1*, 16064; d) Y. Jiao, Y. Zheng, M. Jaroniec, S. Z. Qiao, *Chem. Soc. Rev.* **2015**, *44*, 2060-2086; e) J. Dombrovskis, A. Palmqvist, *Fuel Cells* **2016**, *16*, 4-22; f) J. Gao, J. Cong, Y. Wu, L. Sun, J. Yao, B. Chen, *ACS Appl. Energy Mater.* **2018**, *1*, 5140-5144; g) H. Qi, J. Wolfe, D. Wang, H. J. Fan, D. Fichou, Z. Chen, *Nanoscale* **2014**, *6*, 13457-13462; h) S. Tang, X. Wang, Y. Zhang, M. Courte, H. J. Fan, D. Fichou, *Nanoscale* **2019**, DOI: 10.1039/C8NR07787H.

[2] A. Eftekhari, *Mater. Today Energy* **2017**, *5*, 37-57.

[3] a) I. Roger, M. A. Shipman, M. D. Symes, *Nat. Rew. Chem.* **2017**, *1*, 0003; b) L. Han, S. Dong, E. Wang, *Adv. Mater.* **2016**, *28*, 9266-9291; c) B. M. Hunter, H. B. Gray, A. M. Müller, *Chem. Rev.* **2016**, *116*, 14120-14136.

[4] a) J. Wang, W. Cui, Q. Liu, Z. Xing, A. M. Asiri, X. Sun, *Adv. Mater.* **2016**, *28*, 215-230; b) X. ZHANG, K.-h. Liu, H. Zhong, F.-l. Meng, J.-M. Yan, Q. Jiang, *Mater. Chem. Front.* **2017**, *1*, 2155-2173; c) A. Sivanantham, P. Ganesan, S. Shanmugam, *Adv. Funct. Mater.* **2016**, *26*, 4661-4672.

[5] a) B. Zhang, X. Zheng, O. Voznyy, R. Comin, M. Bajdich, M. García-Melchor, L. Han, J. Xu, M. Liu, L. Zheng, *Science* **2016**, *352*, 333-337; b) P. Xiao, X. Ge, H. Wang, Z. Liu, A. Fisher, X. Wang, *Adv. Funct. Mater.* **2015**, *25*, 1520-1526.

[6] a) Y. Zhang, S. Yuan, G. Day, X. Wang, X. Yang, H.-C. Zhou, *Coord. Chem. Rev.* **2017**, *354*, 28-45; b) Y. J. Cui, B. Li, H. J. He, W. Zhou, B. L. Chen, G. D. Qian, *Acc. Chem. Res.* **2016**, *49*, 483-493; c) Y. J. Cui, B. L. Chen, G. D. Qian, *Coord. Chem.*

Rev. **2014**, *273*, 76-86; d) H. Xu, Y. Dong, Y. Wu, W. Ren, T. Zhao, S. Wang, J. Gao, *J. Solid State Chem.* **2018**, *258*, 441-446; e) H. Xu, J. Gao, X. Qian, J. Wang, H. He, Y. Cui, Y. Yang, Z. Wang, G. Qian, *J. Mater. Chem. A* **2016**, *4*, 10900-10905.

[7] a) E. D. Bloch, W. L. Queen, R. Krishna, J. M. Zadrozny, C. M. Brown, J. R. Long, *Science* **2012**, *335*, 1606-1610; b) C. A. Trickett, A. Helal, B. A. Al-Maythalony, Z. H. Yamani, K. E. Cordova, O. M. Yaghi, *Nat. Rev. Mater.* **2017**, *2*, 17045; c) R.-B. Lin, H. Wu, L. Li, X.-L. Tang, Z. Li, J. Gao, H. Cui, W. Zhou, B. Chen, *J. Am. Chem. Soc.* **2018**, *140*, 12940-12946.

[8] a) C. Doonan, R. Riccò, K. Liang, D. Bradshaw, P. Falcaro, *Acc. Chem. Res.* **2017**, *50*, 1423-1432; b) Z. Dong, Y. Sun, J. Chu, X. Zhang, H. Deng, *J. Am. Chem. Soc.* **2017**, *139*, 14209-14216; c) M. Giménez-Marqués, T. Hidalgo, C. Serre, P. Horcajada, *Coord. Chem. Rev.* **2016**, *307*, 342-360.

[9] a) R. Medishetty, J. K. Zaręba, D. Mayer, M. Samoć, R. A. Fischer, *Chem. Soc. Rev.* **2017**, *46*, 4976-5004; b) I. Stassen, N. Burtch, A. Talin, P. Falcaro, M. Allendorf, R. Ameloot, *Chem. Soc. Rev.* **2017**, *46*, 3185-3241.

[10] a) L. Zhu, X.-Q. Liu, H.-L. Jiang, L.-B. Sun, *Chem. Rev.* **2017**, *117*, 8129-8176; b) K. Shen, L. Zhang, X. Chen, L. Liu, D. Zhang, Y. Han, J. Chen, J. Long, R. Luque, Y. Li, *Science* **2018**, *359*, 206-210; c) Y.-B. Huang, J. Liang, X.-S. Wang, R. Cao, *Chem. Soc. Rev.* **2017**, *46*, 126-157; d) A. Dhakshinamoorthy, A. M. Asiri, H. García, *Angew. Chem. Int. Ed.* **2016**, *55*, 5414-5445; e) W. Ren, J. Gao, C. Lei, Y. Xie, Y. Cai, Q. Ni, J. Yao, *Chem. Eng. J.* **2018**, *349*, 766-774; f) J. Gao, J. Miao, P.-Z. Li, W. Y. Teng, L. Yang, Y. Zhao, B. Liu, Q. Zhang, *Chem. Commun.* **2014**, *50*, 3786-3788.

[11] a) P.-Q. Liao, J.-Q. Shen, J.-P. Zhang, *Coord. Chem. Rev.* **2018**, *373*, 22-48; b) Y.-Z. Chen, R. Zhang, L. Jiao, H.-L. Jiang, *Coord. Chem. Rev.* **2018**, *362*, 1-23; c) H. Wang, Q.-L. Zhu, R. Zou, Q. Xu, *Chem* **2017**, *2*, 52-80; d) Y. V. Kaneti, J. Tang, R. R. Salunkhe, X. Jiang, A. Yu, K. C. W. Wu, Y. Yamauchi, *Adv. Mater.* **2017**, *29*, 1604898; e) S. Dang, Q.-L. Zhu, Q. Xu, *Nat. Rev. Mater.* **2017**, *3*, 17075; f) R. R. Salunkhe, Y. V. Kaneti, J. Kim, J. H. Kim, Y. Yamauchi, *Acc. Chem. Res.* **2016**, *49*, 2796-2806.

[12] a) S. Liu, J. Li, X. Yan, Q. Su, Y. Lu, J. Qiu, Z. Wang, X. Lin, J. Huang, R. Liu, *Adv. Mater.* **2018**, *30*, 1706895; b) K. Qu, Y. Zheng, X. Zhang, K. Davey, S. Dai, S. Z. Qiao, *ACS Nano* **2017**, *11*, 7293-7300; c) J. Yang, X. Zhou, D. Wu, X. Zhao, Z. Zhou, *Adv. Mater.* **2017**, *29*, 1604108.

[13] a) S. K. Misra, I. Srivastava, I. Tripathi, E. Daza, F. Ostadhossein, D. Pan, *J. Am. Chem. Soc.* **2017**, *139*, 1746-1749; b) D. Y. Chung, S. W. Jun, G. Yoon, H. Kim, J. M. Yoo, K.-S. Lee, T. Kim, H. Shin, A. K. Sinha, S. G. Kwon, *J. Am. Chem. Soc.* **2017**, *139*, 6669-6674; c) F. Zheng, Y. Yang, Q. Chen, *Nat. Commun.* **2014**, *5*, 5261.

[14] a) Y. Pei, Z. Qi, X. Li, R. V. Maligal-Ganesh, T. W. Goh, C. Xiao, T. Wang, W. Huang, *J. Mater. Chem. A* **2017**, *5*, 6186-6192; b) W. Zhang, X. Jiang, Y. Zhao, A. Carné-Sánchez, V. Malgras, J. Kim, J. H. Kim, S. Wang, J. Liu, J.-S. Jiang, *Chem. Sci.* **2017**, *8*, 3538-3546; c) Y. Han, Y.-G. Wang, W. Chen, R. Xu, L. Zheng, J. Zhang, J. Luo, R.-A. Shen, Y. Zhu, W.-C. Cheong, *J. Am. Chem. Soc.* **2017**, *139*, 17269-17272; d) Y. M. Chen, L. Yu, X. W. D. Lou, *Angew. Chem. Int. Ed.* **2016**, *55*, 5990-5993; e) Y. Wu, M. Lu, Y. Li, P. He, S. B. Maddine, J. Gao, J. Yao, *Chem. Asian J.* **2018**, *13*, 3274-3280.

[15] a) P. Pachfule, D. Shinde, M. Majumder, Q. Xu, *Nat. Chem.* **2016**, *8*, 718; b) X. Wan, R. Wu, J. Deng, Y. Nie, S. Chen, W. Ding, X. Huang, Z. Wei, *J. Mater. Chem. A* **2018**, *6*, 3386-3390; c) W. Zhang, X. Jiang, X. Wang, Y. V. Kaneti, Y. Chen, J. Liu, J. S. Jiang, Y. Yamauchi, M. Hu, *Angew. Chem. Int. Ed.* **2017**, *56*, 8435-8440; d) J. Meng, C. Niu, L. Xu, J. Li, X. Liu, X. Wang, Y. Wu, X. Xu, W. Chen, Q. Li, *J. Am. Chem. Soc.* **2017**, *139*, 8212-8221.

[16] a) J. Zhou, Y. Dou, A. Zhou, R. M. Guo, M. J. Zhao, J. R. Li, *Adv. Energy Mater.* **2017**, *7*, 1602643; b) Y. Xu, W. Tu, B. Zhang, S. Yin, Y. Huang, M. Kraft, R. Xu, *Adv. Mater.* **2017**, *29*, 1605957; c) H. B. Wu, X. W. D. Lou, *Sci. Adv.* **2017**, *3*, eaap9252.

[17] F. Wang, Z. S. Liu, H. Yang, Y. X. Tan, J. Zhang, *Angew. Chem. Int. Ed.* **2011**, *50*, 450-453.

[18] J. Cong, H. Xu, M. Lu, Y. Wu, Y. Li, P. He, J. Gao, J. Yao, S. Xu, *Chem. Asian J.* **2018**, *13*, 1485-1491.

[19] a)Y. Qin, J. Yuan, J. Li, D. Chen, Y. Kong, F. Chu, Y. Tao, M. Liu, *Adv. Mater.* **2015**, *27*, 5171-5175; b) J. Wang, J. Cong, H. Xu, J. Wang, H. Liu, M. Liang, J. Gao, Q. Ni, J. Yao, *ACS Sustain. Chem. Eng.* **2017**, *5*, 10633-10639; c) J. Wang, H. Xu, X. Qian, Y. Dong, J. Gao, G. Qian, J. Yao, *Chem. Asian J.* **2015**, *10*, 1276-1280.

[20] X. Yang, Y. C. Kimmel, J. Fu, B. E. Koel, J. G. Chen, *ACS Catal.* **2012**, *2*, 765-769.

[21] a) S. Meyer, A. V. Nikiforov, I. M. Petrushina, K. Köhler, E. Christensen, J. O. Jensen, N. J. Bjerrum, *Int. J. Hydrogen Energy* **2015**, *40*, 2905-2911; b) P. D. Tran, S. Y. Chiam, P. P. Boix, Y. Ren, S. S. Pramana, J. Fize, V. Artero, J. Barber, *Energy Environ. Sci.* **2013**, *6*, 2452-2459.

[22] B. You, N. Jiang, M. Sheng, S. Gul, J. Yano, Y. Sun, *Chem. Mater.* **2015**, *27*, 7636-7642.

[23] L. Jiao, Y.-X. Zhou, H.-L. Jiang, *Chem. Sci.* **2016**, *7*, 1690-1695.

[24] L. L. Feng, G. Yu, Y. Wu, G. D. Li, H. Li, Y. Sun, T. Asefa, W. Chen, X. Zou, *J. Am. Chem. Soc.* **2015**, *137*, 14023-14026.

[25] M. Ledendecker, S. Krick Calderon, C. Papp, H. P. Steinruck, M. Antonietti, M. Shalom, *Angew. Chem. Int. Ed.* **2015**, *54*, 12361-12365.

[26] J. Li, M. Wan, T. Li, H. Zhu, Z. Zhao, Z. Wang, W. Wu, M. Du, *Electrochim. Acta* **2018**, *272*, 161-168.

[27] N. Jiang, B. You, M. Sheng, Y. Sun, *Angew. Chem. Int. Ed.* **2015**, *54*, 6251-6254.

[28] W. Lu, T. Liu, L. Xie, C. Tang, D. Liu, S. Hao, F. Qu, G. Du, Y. Ma, A. M. Asiri, X. Sun, *Small* **2017**, *13,* 1700805.

[29] H. Jin, J. Wang, D. Su, Z. Wei, Z. Pang, Y. Wang, *J. Am. Chem. Soc.* **2015**, *137*, 2688-2694.

[30] R. Xu, R. Wu, Y. Shi, J. Zhang, B. Zhang, *Nano Energy* **2016**, *24*, 103-110.

Table of Contents Only

Nanoscale MOFs are successfully synthesized via a microwave method and is used o produce porous nitrogen-doped carbon materials encapsulating cobalt and tungsten carbide (Co/W-C@NCNSs). The obtained Co/W-C@NCNSs exhibit superior performance towards both the OER and HER in alkaline media.

Keyword: metal-organic frameworks; electrocatalysis; carbon materials; oxygen evolution reaction; hydrogen evolution reaction

T. Zhao[a], J. Gao[a,b*], J. Wu[a], P. He[a], Y. Li[a], J. Yao[a]

Highly active cobalt/tungsten carbide@N-doped porous carbon nanomaterials derived from metal-organic frameworks as bifunctional catalysts for overall water splitting